






Effect of the Materials' Properties in the Design of High Transmittance and Low FWHM SiO₂/TiO₂ Thin Film Optical Filters for Integration in a Malaria Diagnostics Device

Mariana S. Costa¹^a, Vitória Baptista^{1,2,3}^b, Graça Minas¹^c, Maria I. Veiga^{2,3}^d
and Susana O. Catarino¹^e

¹*Microelectromechanical Systems Research Unit (CMEMS-UMinho), School of Engineering, University of Minho, Campus de Azurém, Guimarães, Portugal*

²*Life and Health Sciences Research Institute (ICVS), School of Medicine, University of Minho, Campus de Gualtar, Braga, Portugal*

³*ICVS/3B's – PT Government Associate Laboratory, Braga/ Guimarães, Portugal*

Keywords: Malaria Diagnostics Device, Optical Filters, Optical Reflectance, Refractive Index, TFCalc.


Abstract: Malaria is an infectious disease, highly prevalent in world regions with lacking healthcare conditions. Nowadays, malaria diagnostic methods in these endemic regions are mainly based on microscopy and rapid diagnostic tests by immunochromatographic assays. Here, it is presented an optical diagnostic method, based on reflectance spectrophotometry, through hemozoin (Hz) quantification, towards an innovative non-invasive malaria diagnostic device. Therefore, a set of optical filters, with high transmittance and low full width at half maximum (FWHM) at specific wavelengths, is designed for being integrated in the device. These allow the full reconstruction of the optical reflectance spectrum, able to distinguish between healthy and infected samples, with a detection limit up to 12.5 parasites/ μ l of red blood cells. This work presents the design, performance simulation, and optimization of 16 highly selective narrow band-pass optical filters, based on multilayer stacks of SiO₂/TiO₂ thin films. The optical properties of the thin films layer materials, in particular the refractive indexes, are the main focus in this study. Three different reflective indexes were evaluated and the results showed that, for all the simulated conditions, each filter is sensitive to a single wavelength with a FWHM < 25 nm and peak transmittance intensity > 90%, but slight variations were observed for the different refractive indexes. The simulation results proved that these 16 optical filters designs are extremely sensitive to the material properties, although they are the best option regarding the required optical response, assuring feasibility and being adequate for the fabrication process.


1 INTRODUCTION


Malaria is a life-threatening and parasitic infectious disease, with a worldwide impact. This disease is a leading cause of death in many malaria-endemic regions such as Western Pacific, South, and Central America, sub-Saharan Africa, South East Asia, and the Eastern Mediterranean. Simultaneously, malaria imported infections, in non-endemic areas amongst returning travellers from endemic regions, are


significantly increasing. In 2018, there were still 87 countries and regions with ongoing malaria transmission, and malaria resulted in an estimated 228 million cases and 405 000 deaths (Mer et al., 2020).


Nowadays, there are available many methods for malaria diagnosis, which are based on the detection of the parasites in the blood. Examples of these methods are clinical diagnosis, optical microscopy, molecular diagnosis by polymerase chain reaction

^a <https://orcid.org/0000-0001-8519-0525>

^b <https://orcid.org/0000-0002-4895-8053>

^c <https://orcid.org/0000-0003-2460-0556>

^d <https://orcid.org/0000-0002-2205-8102>

^e <https://orcid.org/0000-0002-8962-0710>

(PCR) or loop-mediated isothermal amplification (LAMP) and, more recently, several commercially available rapid diagnostic tests (RDT). Clinical diagnosis is the traditional method, based on the analysis of the patients' symptoms, which is performed by a medical specialist. Therefore, the risk associated with the subjectivity of this method may lead to misdiagnosis and wrong treatment (Orish et al., 2016). Optical microscopy allows the quantification and distinction of species but requires laboratorial equipment and qualified technicians, which can lead to a subjective interpretation of the results. This method is inexpensive yet difficult to implement in remote endemic regions, allowing for a detection limit between 50 to 100 parasites/ μl of red blood cells (Kasetsirikul et al., 2016). RDT have comparable sensitivity and can be used in remote locations. However, RDT are expensive and do not allow the quantification of parasites, only allowing their identification. The detection limit of this method is 100 parasites/ μl of red blood cells (Varo et al., 2020). In terms of sensitivity and specificity, the best method is the molecular diagnosis using PCR or LAMP, with a detection limits of 1 to 5 parasites/ μl and ≤ 1 parasites/ μl of red blood cells, respectively. Nevertheless, these techniques need to be performed in equipped laboratories. Thus, they are not used as routine diagnosis on the field, being applied only for research purposes (Gitta et al., 2020). Since all these methods require the collection of blood samples and disposable reagents and/or consumables (Silva et al., 2017), new portable and low-cost diagnosis methods and devices have been developed, aiming for innovative solutions with no need for blood samples and, therefore, non-invasive.

The malaria disease is caused by *Plasmodium* parasites that are transmitted to humans via the bite of infected female *Anopheles* mosquito vectors. If the disease is not treated timely, progression to severe disease with organ dysfunction and death may occur (Krampa et al., 2020). The presence of malaria parasites on human blood leads to a set of morphological and biochemical alterations on the red blood cells (RBCs). One of the main phenomena is the degradation of haemoglobin (Hb), which is an essential nutrient for *Plasmodium* metabolism during its intracellular development. Hb degradation leads to the release of the toxic heme group. Then, the parasite detoxicates and produces crystal particles of heme, called hemozoin (Hz). Hz, being the final product of the Hb catabolism, accumulates in the RBCs as the infection proliferates, while the Hb concentration decreases. Additionally, human healthy blood does

not have any Hz and its concentration increases as the disease advances.

Since Hz and Hb have different characteristic optical spectra, mainly in the visible range, with different absorbance and reflectance peaks, and those spectra are modified according to the Hb and Hz concentrations in blood (related to the presence or absence of malaria infection), it is possible to identify the presence of malaria parasites through optical reflectance spectrophotometry as well as predict the infection stage (Baptista et al., 2020; Catarino et al., 2020; Silva et al., 2017).

Therefore, optical spectrophotometry, based on absorbance or reflectance, has been arising as an alternative solution for the improvement of the existing malaria diagnostic methods and devices. (Wong Kee Song, 2005). The research team proposes the implementation of a non-invasive optical device based on optical reflectance for the identification and quantification of malaria parasites, aiming for a detection limit up to 12.5 parasites/ μl of red blood cells. The device must contain optical band-pass filters, specific for selected wavelengths, with high transmittance and low full width at half maximum (FWHM), to allow the reconstruction of the optical reflectance spectra of the samples from a set of discrete reflectance values. The optical device will include a white light source, that emits light directed to the sample, since the reflected sample's spectrum contains the specificity of the sample composition. This reflected light reaches an array of photodiodes, which converts the reflected light into electric currents. The designed optical filters (16 filters, as will be following detailed) will be responsible for selecting and filtering the light at different wavelengths, helping to reconstruct the spectrum of each sample. Also, these filters must be multilayer thin films, able to be deposited, during fabrication, on top of a 16 silicon photodiodes' array, included in the optical device. Since it is well-known that thin-film optical filters are highly sensitive to the properties of their materials, as well as their thickness, the main motivation for this work is to study the spectral response of different dielectric materials, with different optical properties, aiming for their full characterization before fabrication. Therefore, in this work, the spectral response of 16 thin-film band-pass optical filters will be simulated, considering different refractive indexes (from different databases), and their performance will be assessed and discussed.

2 DESIGN OF THIN-FILM OPTICAL FILTERS

Figure 1 presents the original continuous reflectance spectra of healthy RBCs and parasite infected RBCs, at different parasitaemia, measured with a spectrophotometric top-bench setup, comprised by a 200 W Quartz Tungsten Halogen light source (model 66881, Oriol Newport), optical-fibre probes, a cuvette sample holder and an AvaSpec-ULS2048XL EVO spectrometer (Avantes). Data were collected using the AvaSoft 8.11 software. Barium sulphate was used as a reference for reflectance measurements. The *plasmodium falciparum* samples were cultured at Life and Health Sciences Research Institute from University of Minho (ICVS) (Baptista et al., 2020).

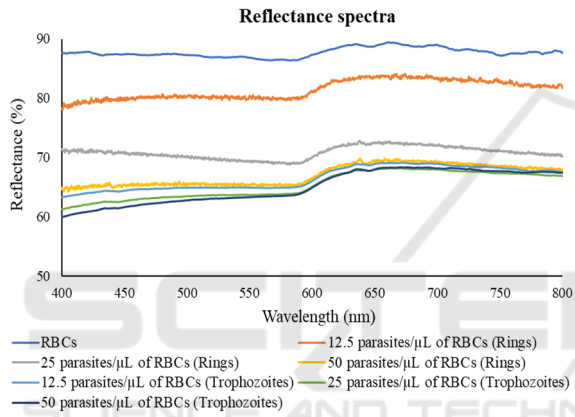


Figure 1: Reflectance spectra of healthy RBCs and RBCs with early (rings) and late (trophozoites) with different parasitaemia, from 12.5 to 50 parasites/all of the RBCs.

From this previous work of the research group (Baptista et al., 2020) (represented in Figure 1), it was selected a group of 16 specific relevant spectral bands, in the optical spectrum. This set of wavelengths will allow to reconstruct the continuous reflectance spectra of the samples, containing healthy RBCs and RBCs with early (rings) and late (trophozoites) with parasitaemia ranging from 12.5 to 50 parasites/RBCs (Baptista et al., 2020). These selected spectral bands are: 400, 435, 520, 590, 610, 620, 630, 640, 650, 660, 670, 680, 700, 720, 740 and 800 nm. In the following section, the methods for the design of 16 thin-film multilayer optical filters for the above referred narrow spectral bands will be described.

2.1 Multilayer Structure Selection

The proposed narrow band-pass optical filters are based on a multilayer thin-film structure, taking advantage of the constructive or destructive combinations that produce, simultaneously, passing and rejection optical bands. The filters' structures are similar to a Fabry-Perot interferometer structure, which consists of two flat parallel mirrors separated by a layer with a pre-defined thickness, called resonance cavity (Minas et al., 2004).

Figure 2 presents the working principle of a multilayer optical filter, where the multilayer structure, composed by two parallel mirrors and visible resonance cavity, is visible. According to the literature in the optical field, to obtain a good filter performance using a Fabry-Perot interferometer structure, the total number of layers must be 9 or 11. After the simulations, it was chosen the 11 layers per filter structure (Minas et al., 2006). The mirrors can be dielectric films, featuring low energy absorption rates and high transmittance at specific wavelengths, comprised by five layers each with, alternatively, high (H) and low (L) refractive index materials. The resonance cavity of the filter has a multiple-beam interference that causes a very high optical transmission at a narrow band of wavelengths around a wavelength for which the cavity is a multiple of one-half wavelength thick. Furthermore, considering a simple approach for the design of the optical filters (an interference of first order and a light incidence angle of 0°), Figure 2 presents two expressions for the calculation of the resonance cavity and mirror thicknesses, d_t and d_s , respectively. Finally, λ is the transmitted wavelength and n is the refractive index of the resonant cavity material (Pimenta et al., 2015).

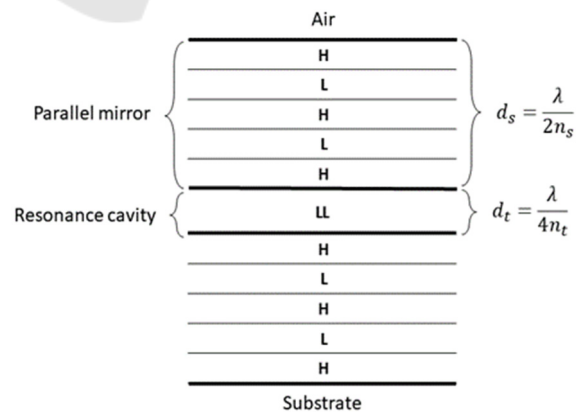


Figure 2: Multilayer optical filter structure.

Therefore, in this optical filter structure, considering similar films on both mirrors, the thickness of the resonance cavity determines the tuned wavelength. Taking advantage of that, 16 filters were computationally designed and simulated using the TFCalc 3.5 software, based on finite elements methods, and supplied by Software Spectra Inc. As previously referred, those filters were centred at 16 specific spectral bands in the visible optical spectrum: 400, 435, 520, 590, 610, 620, 630, 640, 650, 660, 670, 680, 700, 720, 740 and 800 nm.

2.2 Materials Selection

The parallel mirrors of the Fabry-Perot optical filters are composed by multilayer stacks made with dielectric thin films, which can produce high transmission and low absorption losses. Since the multilayer structure should consist in thin films with low and high refractive indexes, silicon dioxide (SiO_2) and titanium dioxide (TiO_2), with low and high refractive indexes, respectively, were selected as the materials to comprise the filters. These dielectrics materials are rigid, extremely difficult to remove from the substrate, compatible with CMOS fabrication and commonly deposited by Ion Beam Deposition (IBD), which is the process typically used for fabrication of optical filters. Additionally, SiO_2 was selected because of its almost constant dependence of the refractive index, within the visible range in the light spectrum, while TiO_2 was selected due to fabrication constraints since its deposition process is well-characterized (Pimenta et al., 2015).

3 SIMULATION OF THIN FILMS OPTICAL FILTERS

Regarding the simulations, the TFCalc 3.5 software was used for the computational design and simulation of the 16 optical filters, characterizing them in terms of transmittance peak and FWHM. The intensity of the transmitted peaks should be as high as possible, with at least twice the intensity of any noise peak that might appear in the considered spectral range. Regarding the FWHM, a value around 10 nm is acceptable for the intended application.

In order to optimize the design and future fabrication processes, the optical filters were initially divided into three spectral regions: UV/VIS (400 nm – 435 nm), VIS (520 nm – 620 nm) and VIS/IR (620 nm – 800 nm). In order to centre the optical filters at different spectral bands by adjusting only the

thickness of the resonant cavity, made from SiO_2 , the thicknesses of both mirrors' films were maintained equally. The reference wavelengths chosen for each region were 420 nm, 550 nm and 680 nm, respectively. Besides the properties of the films' materials, the simulation also considered the properties of the substrate (glass), exit medium (glass), reference wavelength, and incident medium (air), which may influence the filters optical response.

In this way, three different experiments of numerical simulations were performed, to assess the best performance of the 16 optical filters, which most closely resembles the performance of the filters that will be achieved after fabrication. Between the different sets of simulations, the values of the refractive indexes (n) of the multilayer materials (SiO_2 and TiO_2) were modified, and different material databases were evaluated. Table 1 presents the refractive indexes of SiO_2 and TiO_2 at the 16 expected spectral bands, according to two databases (*Sopra S.A.* and *refractiveindex.info* (DeVore, 1951; "https://refractiveindex.info/," n.d.; Malitson, 1965), as it will be explained in the following sections.

3.1 Ideal Refractive Indexes

The first design and simulations were performed using the refractive indexes provided by the SOPRA database (Table 1), since these values are considered ideal for both materials, and only depend on the optical wavelength. The *Sopra S.A.* company (France) made its optical database available, as well as the conversion to TFCalc format (Baptista et al., 2020).

Table 2 shows the combination of layer thickness for each optical filter designed in TFCalc, optimized for the highest transmittance, for each relevant wavelength. As observed in the table, the narrow optical filters were divided into four regions: 400 – 435 nm, 520 – 620 nm, 630 – 720 nm and 740 – 800 nm, each group with similar layer thicknesses for the mirrors, which will facilitate the design of masks and future fabrication of the thin film optical filters.

In the designed filters, the two mirrors are symmetrical and consist of five layers of TiO_2 and SiO_2 , alternately, where layers of the same material have the same thickness for each wavelength. This separation of the 16 wavelengths in four sections will be repeated in the next sets of simulations. Finally, for each wavelength, the resonance cavity has a different thickness, which was adjusted to achieve the highest possible optical transmittance.

Table 1: Refractive indexes of SiO₂ and TiO₂ according to Sopra S.A. and *refractiveindex.info* databases.

Wavelength	Refractive Index (<i>n</i>)			
	SiO ₂		TiO ₂	
	<i>Sopra S.A.</i>	<i>refractiveindex.info</i>	<i>Sopra S.A.</i>	<i>refractiveindex.info</i>
400	1.4701	1.4841	3.2861	2.3379
435	1.4668	1.4810	3.2192	2.2690
520	1.4613	1.4759	3.0000	2.1824
590	1.4584	1.4733	2.9100	2.1456
610	1.4577	1.4727	2.8894	2.1379
620	1.4574	1.4724	2.8800	2.1344
630	1.4571	1.4722	2.8750	2.1311
640	1.4568	1.4719	2.8700	2.1280
650	1.4565	1.4717	2.8600	2.1251
660	1.4563	1.4715	2.8500	2.1223
670	1.4560	1.4713	2.8444	2.1197
680	1.4558	1.4711	2.8400	2.1172
700	1.4553	1.4707	2.8300	2.1126
720	1.4549	1.4703	2.8200	2.1084
740	1.4544	1.4700	2.8100	2.1046
800	1.4533	1.4692	2.7900	2.0951

Table 2: Optical filters in the UV/Vis, Vis and Vis/IR regions and respective layer thicknesses, with the combinations SiO₂/TiO₂ using SOPRA refractive index (RC: Resonance Cavity).

Peak of high transmittance per λ (nm)																
	400	435	520	590	610	620	630	640	650	660	670	680	700	720	740	800
Layer thickness (nm)																
TiO ₂	33		46				60					70				
SiO ₂	73		94				117					121				
TiO ₂	33		46				60					70				
SiO ₂	73		94				117					121				
TiO ₂	33		46				60					70				
SiO ₂ (RC)	127	151	168	219	235	243	196	204	211	219	226	233	247	262	248	291
TiO ₂	33		46				60					70				
SiO ₂	73		94				117					121				
TiO ₂	33		46				60					70				
SiO ₂	73		94				117					121				
TiO ₂	33		46				60					70				

3.2 Approximation of the Real Refractive Indexes

Then, a new group of 16 filters was designed and simulated, using the refractive indexes of the materials obtained from the *refractiveindex.info* database. This database is considered closer to the real values of the refractive indexes of the materials, contrarily to the ideal values from *Sopra S.A.*

Table 3 shows the combination of the layer thickness values for each optical filter designed in TFCalc, optimized for the highest transmittance, using the *refractiveindex.info* database.

In comparison with Table 2, it is possible to verify that these refractive indexes values lead to an increase on the thickness of almost all filters (selected to achieve the highest transmittance at the intended wavelengths). However, in the 400 nm and 435 nm band-pass filters, the SiO₂ layer is similar to the

previous one, while in the 630 nm and 800 nm band-pass filters, those thicknesses decrease.

3.3 Impact of the Layer Thickness on the Refractive Indexes of the Materials

Finally, a group of 16 optical filters was designed considering the variation of the refractive index of the

materials (TiO₂ and SiO₂) with the thickness of each layer (Table 4). In this set of simulations, the refractive indexes were gathered from interpolation of the data obtained from previous studies of the research group (Pimenta et al., 2015), where the refractive index of each material was experimentally measured for a specific layer thickness. In the reported data, each refractive index slightly decreases with the increase of wavelength (in the 400 nm – 800

Table 3: Optical filters in the UV/Vis, Vis and Vis/IR regions and respective layer thicknesses, with the combinations SiO₂/TiO₂, using the refractive indexes from *refractiveindex.info* database (RC: Resonance Cavity).

Peak of high transmittance per λ (nm)																
	400	435	520	590	610	620	630	640	650	660	670	680	700	720	740	800
Layer thickness (nm)																
TiO ₂	44		64				78						96			
SiO ₂	73		98				114						120			
TiO ₂	44		64				78						96			
SiO ₂	73		98				114						120			
TiO ₂	44		64				78						96			
SiO ₂ (RC)	125	159	149	218	238	248	192	201	211	218	231	240	260	280	234	293
TiO ₂	44		64				78						96			
SiO ₂	73		98				114						120			
TiO ₂	44		64				78						96			
SiO ₂	73		98				114						120			
TiO ₂	44		64				78						96			

Table 4: Optical filters in the UV/Vis, Vis and Vis/IR regions and respective layer thicknesses, with the combinations SiO₂/TiO₂, using experimental refractive indexes from Pimenta et al. (2016) (RC: Resonance Cavity).

Peak of high transmittance per λ (nm)																
	400	435	520	590	610	620	630	640	650	660	670	680	700	720	740	800
Layer thickness (nm)																
TiO ₂	44		58				70						90			
SiO ₂	73		94				115						120			
TiO ₂	44		58				70						90			
SiO ₂	73		94				115						120			
TiO ₂	44		58				70						90			
SiO ₂ (RC)	114	144	151	211	229	238	185	194	203	211	220	228	245	263	210	262
TiO ₂	44		58				70						90			
SiO ₂	73		94				115						120			
TiO ₂	44		58				70						90			
SiO ₂	73		94				115						120			
TiO ₂	44		58				70						90			

nm range) and is higher as the thickness of the layer increases, for both materials. For example, in the SiO₂ layer, the 73 nm thickness film has refractive indexes around 1.47 (for all wavelengths range, despite their small variations within the optical spectrum), while for the 120 nm thickness film, it has refractive indexes around 1.51. The same happens with the TiO₂ layer, i.e., for a 44 nm thickness, the refractive indexes are between 2.6 and 2.3, while for the 90 nm thickness layers, the refractive indexes are between 2.7 and 2.4, depending on the wavelength.

Therefore, Table 4 presents the combination of the layers' thickness values for each filter, designed in TFCalc, optimized for the highest transmittance when the variation of the refractive index with the thickness is considered.

4 RESULTS AND DISCUSSION

This section presents the main results of the optical filter simulation for the three groups of refractive indexes. The results of each set of designed optical filters simulations are presented through the transmittance spectra for the 16 optical filters.

Figure 3 represents the spectra of the 16 narrow-band optical filters when the SOPRA refractive indexes are considered in the simulations. As seen in Figure 3 plot, the percentage of transmittance is very high (almost 100%) and the FWHM value is lower than 10 nm for all filters. This simulation represents the ideal properties of the materials. However, the resultant spectra will not represent a reliable approximation of the filters' performance after fabrication. Figure 4 presents the simulated spectra of the 16 narrow-band optical filters when refractive

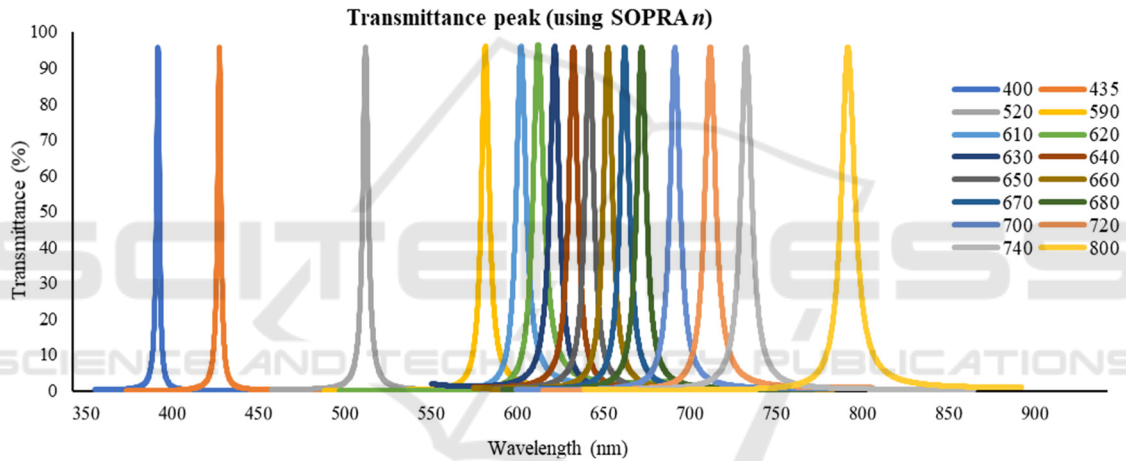


Figure 3: Transmittance vs wavelength, for the matrix of 16 optical filters, using Sopra S.A. refractive indexes. The structure of the filters is shown in Table 2.

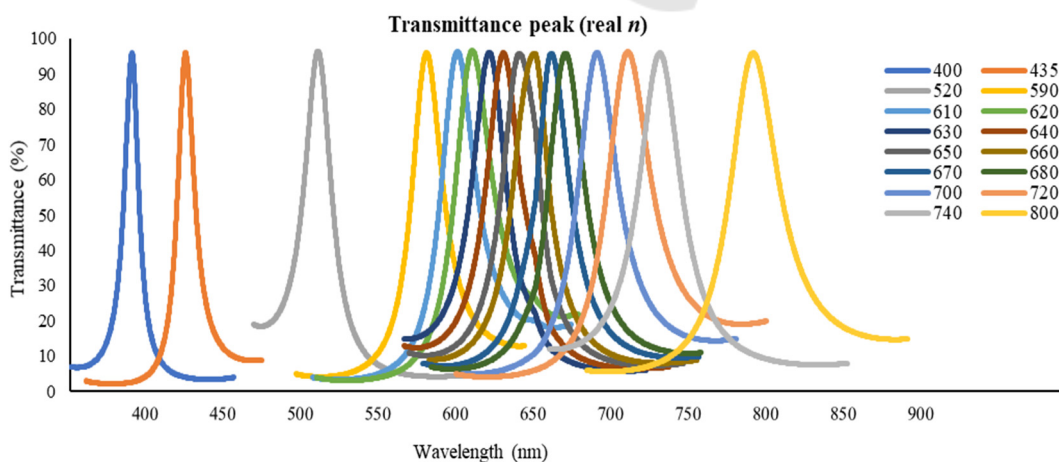


Figure 4: Transmittance vs wavelength, for the matrix of 16 optical filters, using refractive indexes from *refractiveindex.info* database. The structure of the filters is shown in Table 3.

indexes from *refractiveindex.info* database are considered in the simulations.

These results are closer to reality, and describe better the materials' behaviour, which will be essential during fabrication. When compared to the previous results, while the transmittance is still high (> 90%), the FWHM is significantly worse since it is higher than 10 nm for all designed filters.

Finally, Figure 5 presents the spectra of the 16 optical filters, when the refractive index of the thin film materials, used for simulation, is dependent on the thickness of the layer. This design, when compared to the previous one (Figure 4), shows better results regarding the FWHM, since all filters present a FWHM < 10 nm or around this value. Considering the transmittance, their values are above 90%, similarly to the ones from Figure 4.

In all the presented designs, the simulation results confirm that multilayer stacks of 11 layers comprised of SiO₂/TiO₂ thin films and a SiO₂ layer for the resonance cavity are a good option for the design of the thin film and narrow-band optical filters, regarding their optical characteristics. Furthermore, these designs are feasible for future fabrication processes. The performance of the optical filters could be improved by increasing the number of layers in the dielectric mirrors, but the complexity of the fabrication process would also increase (Minas et al., 2004).

Moreover, those simulations allowed to conclude that each band-pass filter for a specific spectral band has a high transmittance, close or exceeding 90% (which is explained by the theoretical refractive indexes), and the FWHM average is around 10 nm when the experimental refractive indexes, dependent on the thickness of the layers, are considered. Additionally, these results show that slight variations

in the refractive indexes imply significant modifications in the thin films filters to achieve high transmittance at the desired spectral band, and this must be taken into account during the fabrication processes.

4.1 Example of Application in the Malaria Parasites Reflectance Spectra

In order to assess if the designed and simulated optical filters would be able to detect differences in optical reflectance spectra, for the intended malaria diagnostics applications, the transmittance data of the designed 16 optical filters (based on the *refractiveindex.info* database) were multiplied by a typical reflectance spectrum of healthy RBCs and by spectra of malaria infected RBCs, at different parasitaemia (spectra previously presented in Figure 1). Figures 6 (a) and (b) present two examples of the spectra obtained from the multiplication between RBCs reflectance spectrum (Figure 1) and all the simulated optical filters transmittance data. Particularly, Figure 6 (a) presents the data for healthy RBCs and Figure 6 (b) presents the data for RBCs with late stage trophozoites containing a parasitaemia of 50 parasites/μl of red blood cells. It is possible to observe that the optical filters spectra are still visible and distinguishable, with slight variations in the peaks' amplitude, resultant from the effect of the reflectance spectra. Finally, Figure 6 (c) presents the spectra resultant from the superposition of the healthy and infected RBCs reflectance spectra with the area of transmittance of all optical filters, i.e., at each wavelength, the plot presents the cumulative effect of all the filters whose transmittance spectra fall on that

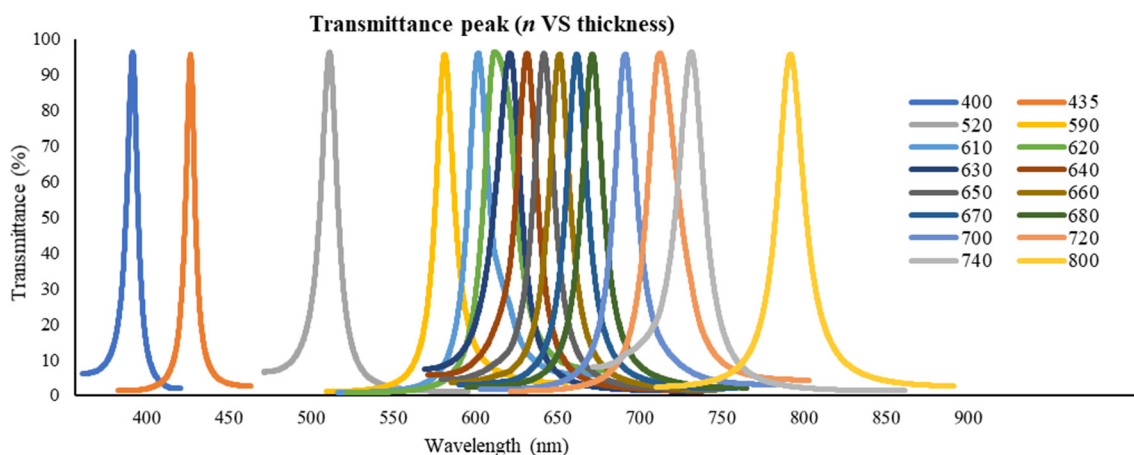


Figure 5: Transmittance vs wavelength, for the matrix of 16 optical filters, using experimental refractive indexes from Pimenta et al. (2016). The structure of the filters is shown in Table 4.

specific wavelength. For instance, while at 435 nm only one filter allows light to be transmitted (the 435 nm filter), at 620 nm, all filters from 590 nm and 640 nm allow some light to be transmitted, increasing the total amount of light to be received by the photodiode array. The high number of optical filters presented in the 570 nm – 750 nm range leads to an increase in the total amplitude of the plot in that region, Figure 6 (c). The results show that, between 400 nm and 550 nm, there is no notorious difference between healthy and malaria-infected RBCs. However, in the 600 nm – 650 nm range, there is a significant increase in the obtained spectra, and the slope between 500 nm and 650 nm is higher as the parasitaemia decreases. From

these results, it is possible to infer that the system may be able to distinguish between healthy and malaria infected samples, enhancing its potential as a diagnostic tool.

5 CONCLUSIONS

The paper describes the design, performance simulation and optimization of 16 narrow band-pass optical filters with multilayers based on thin films of SiO₂/TiO₂, aiming an optical reflectance device for non-invasive malaria diagnostics. These filters were

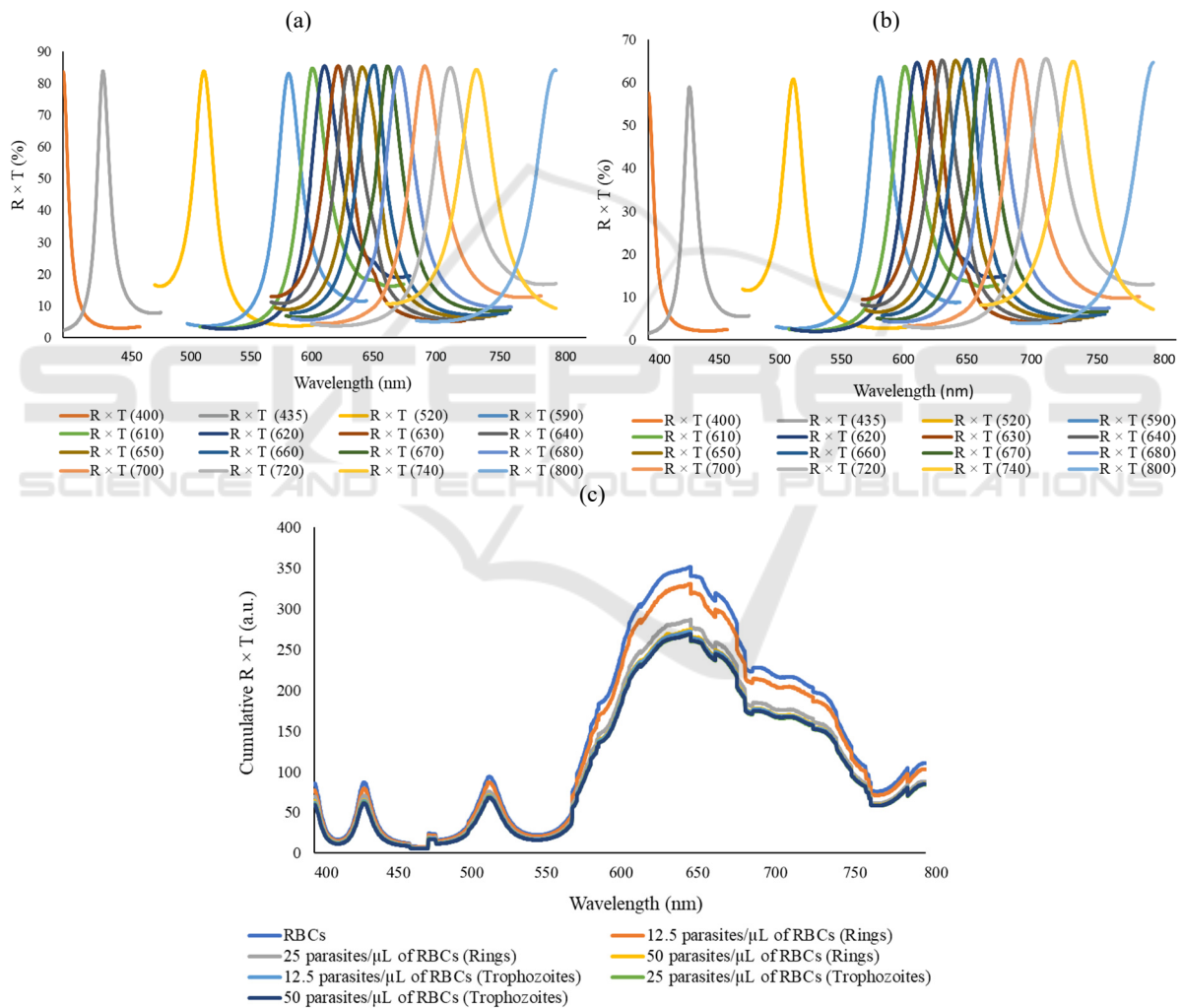


Figure 6: (a) Optical transmittance spectra (%) obtained from the multiplication between the healthy RCBs reflectance spectrum and the optical filters transmittance spectra; (b) Optical transmittance spectra (%) obtained from the multiplication between the RBCs with late stage trophozoites with a parasitaemia of 50 parasites/μl reflectance spectrum and the optical filters transmittance spectra; (c) Optical transmittance spectra (a.u.) resultant from the superposition of the healthy and infected RBCs reflectance spectra (Figure 1) with the area of transmittance of all 16 optical filters.

characterized taking into account the materials of the layers, as well as the requirements for high optical transmittance and low FWHM. The design and simulation of thin-film optical filters are a challenging process. Several variables must be simultaneously controlled to obtain optical filters centred at the desired wavelengths, such as the thin-films' materials, thickness of each layer, refractive indexes of the materials and multilayer structure. Additionally, the simulated results showed that slight variations in the refractive indexes imply significant modifications in the thin films filters to achieve high transmittance at the desired spectral band, a feature that must be taken into account during the fabrication processes. A compromise between the variation of the materials' refractive indexes and the filter's performance was achieved.

Despite some deviations in the simulated results for the different experiments of the optical filters (mainly in the FWHM values), their performance was successfully evaluated, since it is possible to obtain high transmittance for each of the selected wavelengths. Also, the simulation results proved that these 16 optical filters designs are extremely sensitive to the material properties. However, the simulation results also show that these filters are a good option regarding the required optical response, assuring feasibility and being suitable for the fabrication process, showing high potential to be integrated into the intended optical reflectance device for malaria diagnosis.

Finally, the results from the combination of the samples' reflectance and the optical filters' transmittance spectra, also show the potential of the presented system to distinguish between samples of different malaria parasites' concentration with high sensitivity, up to a limit of 12.5 parasites per microliter of RBCs. This value is comparable to current diagnostic methods and detection devices. Besides that, the proposed optical diagnosis methodology device is new, easily implemented, non-invasive and does not need specialised laboratorial equipment or facilities. Following the promising simulation results, future developments will include the deposition processes to fabricate the 16 optical filters.

ACKNOWLEDGEMENTS

This work was supported by Project NORTE-01-0145-FEDER-028178 funded by NORTE 2020 Portugal Regional Operational Program under PORTUGAL 2020 Partnership Agreement through

the European Regional Development Fund and the Fundação para a Ciência e Tecnologia (FCT), IP. V. Baptista thanks FCT for the SFRH/BD/145427/2019 grant. Maria Isabel Veiga thanks FCT for her contract funding provided through DL 57/2016 (CRP).

REFERENCES

- Baptista, V., Calçada, C., Silva, M., Teixeira, M., Ferreira, P., Minas, G., ... Veiga, M. (2020). Hemozoin: the future in malaria diagnosis. *MAM 2020 – Molecular Approaches to Malaria, Lorne, Australia*, 28178.
- Catarino, S. O., Felix, P., Sousa, P. J., Pinto, V., Veiga, M. I., & Minas, G. (2020). Portable Device for Optical Quantification of Hemozoin in Diluted Blood Samples. *IEEE Transactions on Biomedical Engineering*, 67(2), 365–371. <https://doi.org/10.1109/TBME.2019.2913454>
- DeVore, J. R. (1951). Refractive Indices of Rutile and Sphalerite. *Journal of the Optical Society of America*, 41(6), 416. <https://doi.org/10.1364/josa.41.000416>
- Gitta, B., & Kilian, N. (2020). Diagnosis of Malaria Parasites Plasmodium spp. in Endemic Areas: Current Strategies for an Ancient Disease. *BioEssays*, 42(1), 1–12. <https://doi.org/10.1002/bies.201900138>
- <https://refractiveindex.info/>. (n.d.). Retrieved September 8, 2020, from <https://refractiveindex.info/>
- Kasetsirikul, S., Buranapong, J., Srituravanich, W., Kaewthamasorn, M., & Pimpin, A. (2016). The development of malaria diagnostic techniques: A review of the approaches with focus on dielectrophoretic and magnetophoretic methods. *Malaria Journal*, 15(1). <https://doi.org/10.1186/s12936-016-1400-9>
- Krampa, F. D., Aniwah, Y., Kanyong, P., & Awandare, G. A. (2020). Recent advances in the development of biosensors for malaria diagnosis. *Sensors (Switzerland)*, 20(3). <https://doi.org/10.3390/s20030799>
- Malitson, I. H. (1965). Interspecimen Comparison of the Refractive Index of Fused Silica*,†. *Journal of the Optical Society of America*, 55(10), 1205. <https://doi.org/10.1364/josa.55.001205>
- Mer, M., Dünser, M. W., Giera, R., & Dondorp, A. M. (2020). Severe malaria. Current concepts and practical overview: What every intensivist should know. *Intensive Care Medicine*, 46(5), 907–918. <https://doi.org/10.1007/s00134-020-06019-0>
- Minas, G., Wolffenbuttel, R. F., & Correia, J. H. (2006). An array of highly selective Fabry-Perot optical channels for biological fluid analysis by optical absorption using a white light source for illumination. *Journal of Optics A: Pure and Applied Optics*, 8(3), 272–278. <https://doi.org/10.1088/1464-4258/8/3/008>
- Minas, Graca, Ribeiro, J. C., Martins, J. S., Wolffenbuttel, R. F., & Correia, J. H. (2004). An array of Fabry-Perot optical-channels for biological fluids analysis. *Sensors*

- and Actuators, A: Physical*, 115(2-3 SPEC. ISS.), 362–367. <https://doi.org/10.1016/j.sna.2004.03.077>
- Orish, V. N., Ansong, J. Y., Onyebor, O. S., Sanyaolu, A. O., Oyibo, W. A., & Iriemenam, N. C. (2016). *Overdiagnosis and overtreatment of malaria in children in a secondary healthcare centre in Sekondi-Takoradi, Ghana*. <https://doi.org/10.1177/0049475515622861>
- Pimenta, S., Cardoso, S., Miranda, A., De Beule, P., Castanheira, E. M. S., & Minas, G. (2015). Design and fabrication of SiO₂/TiO₂ and MgO/TiO₂ based high selective optical filters for diffuse reflectance and fluorescence signals extraction. *Biomedical Optics Express*, 6(8), 3084. <https://doi.org/10.1364/boe.6.003084>
- Silva, I., Lima, R., Minas, G., & Catarino, S. O. (2017). Hemozoin and hemoglobin characterization by optical absorption towards a miniaturized spectrophotometric malaria diagnostic system. *ENBENG 2017 - 5th Portuguese Meeting on Bioengineering, Proceedings*, 3–6. <https://doi.org/10.1109/ENBENG.2017.7889466>
- Varo, R., Balanza, N., Mayor, A., & Bassat, Q. (2020). Diagnosis of clinical malaria in endemic settings. *Expert Review of Anti-Infective Therapy*, 0(0). <https://doi.org/10.1080/14787210.2020.1807940>
- Wong Kee Song, L. M. (2005). Optical spectroscopy for the detection of dysplasia in Barrett's esophagus. *Clinical Gastroenterology and Hepatology*, 3(7 SUPPL.), 2–7. [https://doi.org/10.1016/S1542-3565\(05\)00250-8](https://doi.org/10.1016/S1542-3565(05)00250-8)

